Tutorial : The discrete-sectional method to simulate an evolving aerosol

Li, Chenxi

2020-12

Li , C & Cai , R 2020 , ' Tutorial : The discrete-sectional method to simulate an evolving aerosol ' , Journal of Aerosol Science , vol. 150 , 105615 . https://doi.org/10.1016/j.jaerosci.2020.105615

http://hdl.handle.net/10138/324344
https://doi.org/10.1016/j.jaerosci.2020.105615

Journal of Aerosol Science 150 (2020) 105615

Contents lists available at ScienceDirect

Journal of Aerosol Science

journal homepage: http://www.elsevier.com/locate/jaerosci

Tutorial: The discrete-sectional method to simulate an evolving aerosol

Chenxi Li [a], Runlong Cai [b,*]

[a] School of Environmental Science and Engineering, Shanghai Jiao Tong University, Shanghai, 200240, China
[b] Institute for Atmospheric and Earth System Research / Physics, Faculty of Science, University of Helsinki, 00014, Helsinki, Finland

ARTICLE INFO

Keywords:
Aerosol dynamics
Discrete-sectional simulation
General dynamics equations
Particle size distribution
Box model

ABSTRACT

The discrete-sectional method to solve the general dynamic equations is a useful tool for the simulation of an evolving aerosol population. This tutorial is intended to equip the reader with the necessary knowledge to implement this method for a single component system. To this end, we provide step-by-step instructions on the construction of a discrete-sectional model, including details on simulation bin configurations and all the necessary equations to describe relevant physical processes in an aerosol, i.e. condensation/evaporation, coagulation, and external particle losses. Supplementary to the text is a functional, open source MATLAB code that implements the framework introduced in this tutorial. The interested readers can use the code either for learning purposes or to meet research demands. Lastly, we designed six test cases not only to verify the validity of our discrete-sectional model, but also to help the reader gain insight into the evolution of aerosol systems.

1. Introduction

The particle size distribution (PSD) is a basic property of an aerosol population (Seinfeld & Pandis, 2016). Recognizing its importance, a number of aerosol instruments, e.g. scanning mobility particle spectrometer, aerodynamic particle sizer, are dedicated to the measurement of PSD. For a complex aerosol system, the evolution of PSD is often governed by unknown physics/chemistry; therefore, PSDs are routinely simulated parallel to experimental or field observations, with assumptions on aerosol formation, growth, and loss processes. Comparison between the observed and simulated PSDs supports/disapproves the validity of the assumptions, providing insight into the mechanisms behind the observed aerosol evolution (e.g., Kürten et al., 2014). Besides, the simulated PSDs are also used to test the algorithms to characterize aerosol formation, growth, and losses (Li & McMurry, 2018; Vuollekoski, Sihto, Kerminen, Kulmala, & Lehtinen, 2012).

In principle, PSDs can be simulated on the molecular level, assigning one differential equation to describe the evolution of particles with a specific molecular composition. Such a detailed account gets cumbersome very quickly as particle size increases since a particle with a diameter of 1 μm contains $\sim 10^{10}$ molecules and hence at least $\sim 10^{10}$ equations are required for the simulation. Solving such a large number of interrelated differential equations is apparently inefficient; as a result, the sectional method was developed to reduce the number of equations to a manageable level (Gelbard, Tambour, & Seinfeld, 1980), with the central idea that particles within a certain size range (sections) can be approximated by a continuous distribution and described by a single equation. Modifications of the

* Corresponding author.
E-mail address: runlong.cai@helsinki.fi (R. Cai).

https://doi.org/10.1016/j.jaerosci.2020.105615
Received 1 May 2020; Received in revised form 27 May 2020; Accepted 28 May 2020
Available online 26 June 2020

Nomenclature

n_k	number concentration of k-mers, in cm^{-3}
q_k	mass concentration of k-mers, in # of molecules cm^{-3}. The true mass concentration in g cm^{-3} can be calculated by multiplying q_k with molecular mass in g $molecule^{-1}$
N_l	number concentration of particles in bin l, in cm^{-3}
Q_l	mass concentration of particles in bin l, in # of molecules cm^{-3}
S_l	the upper limit of particle mass for section l
L_l	the width of section l, $L_l = S_l - S_{l-1}$
κ	the geometric factor of sections, $\kappa = \frac{S_l}{S_{l-1}}$. κ is set to a constant in this tutorial
$\overline{m}_l$	average mass of particles in section l, $\overline{m}_l = \frac{L_l}{\ln\kappa}$, in # of molecules
ND	number of discrete bins
NS	number of sectional bins
NT	total number of bins, $NT = NS + ND$
$\beta(i,j)$	the collision frequency function between i-mers and j-mers, in $cm^3\ s^{-1}$
R_k	the emission/external production rate of k-mers, in $cm^{-3}\ s^{-1}$
$\dot{Y}_{ij}$	the mass of particles in bin i that coagulate with particles in bin j per unit time, in # of molecules $cm^{-3}\ s^{-1}$
$\dot{Z}_{ij\to u}$	the mass of the coagulation products between bin i and bin j that goes into bin u per unit time, in # of molecules $cm^{-3}\ s^{-1}$
$\overline{C_l}$	average condensation rate coefficient for bin l, in s^{-1}
$\overline{E_l}$:	average evaporation rate coefficient for bin l, in s^{-1}
I_l^+	intersectional mass flux from section l to section l+1 due to condensation, in # of molecules $cm^{-3}\ s^{-1}$
I_l^-	intersectional mass flux from section l to section l-1 due to evaporation, in # of molecules $cm^{-3}\ s^{-1}$
M	dilution rate constant, same for all cluster sizes, in s^{-1}
W_k	wall loss rate constant of k-mers, in s^{-1}
$CoagS_k$	loss rate constant of k-mers to preexisting particles, in s^{-1}

original sectional methods have been proposed to simulate multicomponent systems (Gelbard & Seinfeld, 1980), to better account for condensation/evaporation (Warren & Seinfeld, 1985), or to couple with discrete descriptions for molecular clusters (J. J. Wu & Flagan, 1988). Among these improvements, the coupling of sectional method with discrete equations, referred to as the discrete-sectional method, offers great flexibility in accounting for detailed chemistry/physical processes on the molecular level, while maintaining low computational cost. In modern aerosol research in which the nucleation processes are resolved molecule by molecule (Chen et al., 2012; Lehtipalo et al., 2016), the discrete-sectional approach is particularly useful as researchers try to unravel the detailed mechanisms of the new particle formation processes (Kürten et al., 2018).

In this tutorial, we aim to familiarize readers new to the discrete-sectional method with its basic building blocks. To achieve this goal, we walk the reader through the construction of a discrete-sectional model for a single-component system with detailed specifications on how different physical processes are quantified. Supplied along with this tutorial is a functional, easy-to-implement MATLAB code and several test cases. By working on the test cases the reader can not only become familiar with the model, but also gain insight into the physics of an evolving aerosol. Compared to previous works on the discrete-sectional method, the equations presented in this tutorial is less general in that they are strictly coupled with the bin configurations introduced in section 2.2 and the data structure used in the MATLAB code. We deliberately elected to do so because we are of the opinion that once the reader is familiar with all the details of code writing in one way, it is a relatively simple step to modify the code or build new ones to meet research requirements. Lastly, the model discussed in this tutorial is a 'box model' or '0-dimensional model' because spatial transport terms of mass, momentum and energy are not included. These terms are particularly important in large scale atmospheric simulations (3D models) and simulation of flow reactors (Kommu, Khomami, & Biswas, 2004a; 2004b) but are beyond the scope of this tutorial.

2. Methods

2.1. The general dynamic equations

The evolution of an aerosol can be described by the general dynamic equations (GDE) (Gelbard & Seinfeld, 1979). The GDE is a set of first order differential equations that incorporates physical processes such as condensation, evaporation, coagulation, external particle losses and sources. In this tutorial we consider a spatially homogeneous aerosol, with all the particles composed of molecules (monomers) of the same kind. For simplicity we refer to a particle containing k monomers as k-mer. The rate of change for the number concentrations of monomers is given by

$$\frac{dn_1}{dt} = -n_1\sum_{j=1}^{\infty}\beta_{1,j}n_j + 2E_2n_2 + \sum_{j=3}^{\infty}E_jn_j - EL_1n_1 + R_1 \tag{1}$$

and for k-mers,

$$\frac{dn_k}{dt} = \frac{1}{2}\sum_{i+j=k}\beta_{i,j}n_i n_j \quad - n_k\sum_{j=1}^{\infty}\beta_{k,j}n_j - E_k n_k + E_{k+1}n_{k+1} - EL_k n_k + R_k \ (k \geq 2) \tag{2}$$

where n_k is number concentration (cm^{-3}) of k-mers, $\beta_{i,j}$ is the association rate constant ($cm^3\ s^{-1}$) between i-mer and j-mer, E_k is the rate constants (s^{-1}) for evaporation, EL_k is the external loss rate constant (s^{-1}) and R_k is the external production rate of k-mers ($cm^{-3}\ s^{-1}$). We emphasize that throughout this tutorial as well as in the supplementary code $\beta_{i,j}$ is calculated without the multiplication of 0.5 for i=j (Kruger & Vincenti, 1965). In this way, Eqs. (1) and (2) and subsequent equations automatically take care of bookkeeping of particle numbers as two identical entities collide. Here we also need to clarify some terminology used in this tutorial: we refer to all entities larger than monomer as 'particles', monomer association with monomers and particles as 'condensation', monomer dissociation from particles as 'evaporation', particle-particle association as 'coagulation'. It should be noted that 'condensation' or 'evaporation' is sometimes used to refer to the net rate of monomer association and dissociation (Seinfeld & Pandis, 2016) and the reader should keep the difference in mind.

During coagulation, particle number is not a conserved quantity, i.e. two particles merge into one, but particle mass is. Therefore, it is often convenient to track the particle mass concentration in constructing numerical models. The rate of change for mass concentration of k-mers (q_k , in molecules·cm^{-3}) is given by

$$\frac{dq_k}{dt} = \frac{d(\boldsymbol{k}\cdot n_k)}{dt} = \boldsymbol{k}\cdot\frac{dn_k}{dt} \tag{3}$$

Note in Eq. (3) and throughout this tutorial, *particle mass is given as multiples of monomer mass for convenience.* We do so because we want to use the physically intuitive word 'mass', but at the same time want to keep the equations as simple as possible. As a result, to obtain the true mass concentration of k-mers, q_k needs to be multiplied by the monomer mass.

2.2. Configuration of simulation bins

To numerically solve the GDE, we track the mass concentration variation from monomer up to ND-mer with 'discrete bins', while dividing larger particles into NS 'sectional bins' or 'sections'. Each bin corresponds to an equation hence in total we will solve $NT = ND + NS$ equations. The configuration of simulation bins is graphically illustrated in Fig. 1 for an artificial distribution, with the vertical axis being the particle mass distribution function and the horizontal axis being particle mass expressed in number of molecules contained in the particles. For discrete bins, particle mass is concentrated on discrete points along the mass axis; for sections, particle mass is uniformly distributed within each section, with $q_m dm$ giving the total particulate mass within the mass range between m and $m + dm$ (in sections, both m and q_m are treated as continuous variables). Note that the uniformity of q_m within sections is an assumption we adopt in this tutorial. For a discrete-sectional model, certain assumptions have to be made as to how particles are distributed in sectional bins: it is equally valid (or arbitrary) to assume that particles have uniform number/surface area/mass concentrations within a section and none of these assumptions is perfect. For instance, uniform q_m, when converted to number distribution function by $n_m = \frac{q_m}{m}$, will lead to the inset plot in Fig. 1 with an apparently unphysical number distribution shape. However, the assumption regarding how particles are distributed within sections does not make much difference to the simulation results, as long as the sections are

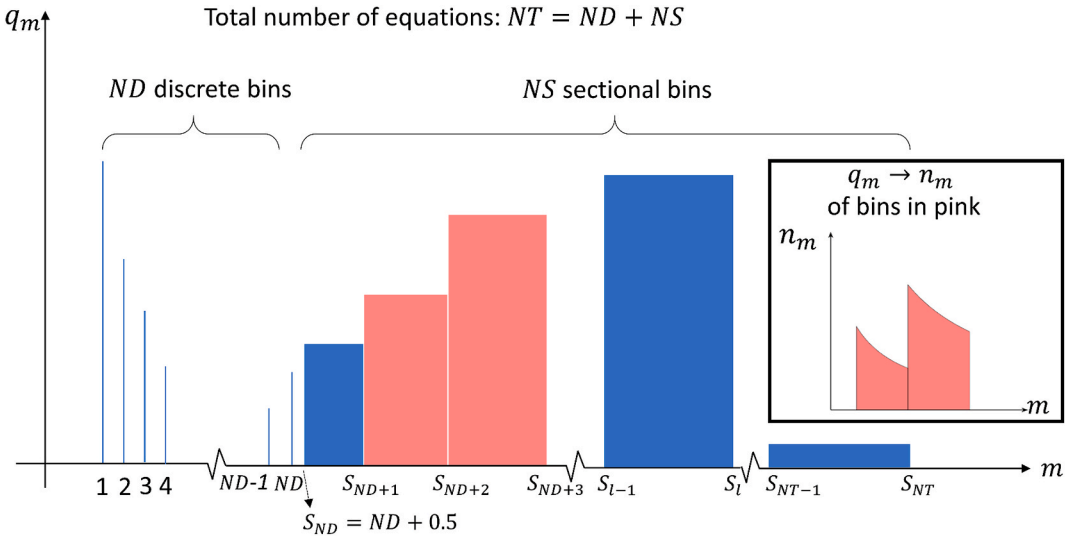

Fig. 1. A graphical illustration of simulation bin configurations in the discrete-sectional model.

sufficiently "narrow" (C. Y. Wu & Biswas, 1998). We will discuss the effect of section width in 3.2.

We use Q_l and N_l to denote the mass and number concentrations of all particles in bin l, be it discrete or sectional. We need to establish a relationship between Q, N, q and n that can be used conveniently in simulations. For discrete bins, their relationship is straightforward,

$$n_l = N_l = \frac{q_l}{l} = \frac{Q_l}{l}, \ (1 \le l \le ND) \tag{4}$$

For sectional bins, Q_l can be calculated by integration,

$$Q_l = \int_{S_{l-1}}^{S_l} q_k \mathrm{d}k = q_k \int_{S_{l-1}}^{S_l} \mathrm{d}k = q_k \cdot L_l, \ k \in (S_{l-1}, \ S_l] \tag{5}$$

where $S_{l\text{-}1}$ and S_l are lower and upper limits of section l, L_l is the section width (equal to $S_l - S_{l-1}$). q_k can be taken out of the integral because of its uniformity in section l. The limits of sections, S_l 's, are often chosen to increase geometrically to facilitate computation. We shall do so in this tutorial, with

$$S_{ND} = ND + 0.5; \ \frac{S_l}{S_{l-1}} = \kappa \tag{6}$$

where S_{ND} is the lower limit for section ND+1, and κ is the ratio between the upper and lower limit for any section, called the *geometric factor*. We can then relate N_l to Q_l by

$$N_l = \int_{S_{l-1}}^{S_l} n_k \mathrm{d}k = \int_{S_{l-1}}^{S_l} \frac{q_k}{k} \mathrm{d}k = \int_{S_{l-1}}^{S_l} \frac{\frac{Q_l}{L_l}}{k} \mathrm{d}k = \frac{Q_l}{L_l} \ln\kappa = \frac{Q_l}{\frac{L_l}{\ln\kappa}} = \frac{Q_l}{\overline{m}_l} \tag{7}$$

In Eq. (7), we define the *average particle mass in section l* as $\overline{m}_l = \frac{L_l}{\ln\kappa}$ so that particle number and mass concentrations in a section are related by a single conversion factor.

Although the sections are usually configured to be log-uniform with a constant κ, non-uniform sections are sometimes used to reduce the simulation errors at the junction between discrete bins and sections. These errors originate from the differences between the discrete and continuous assumptions of the aerosol size distribution. For instance, with $ND = 200$ and $\kappa = 1.0718$, the average particle masses of the last discrete bin and section are 200 and 207.6, respectively. With such a bin configuration, a particle with mass 200 associating with a monomer generates a particle with mass 207.6 in a number-conserving model. Simply reducing κ cannot completely overcome this problem and it may even raise another problem. An extreme example is that when $ND = 200$ and $\kappa = 1.0002$, there will always be no particles in the first section since its mass range is 200.5–200.9. A non-uniform configuration for the first several sections, e.g., using the Fibonacci sequence, may help to reduce these errors, yet we keep the uniform section configuration in this tutorial for its simplicity.

2.3. Solving the GDE

To numerically solve the GDE, we can either calculate $\frac{\mathrm{d}Q_l}{\mathrm{d}t}$ or $\frac{\mathrm{d}N_l}{\mathrm{d}t}$, which are related to each other by Eqs. (4) and (7). In this tutorial we choose to compute $\frac{dQ_l}{dt}$ by quantifying different physical processes separately. The temporal change of Q_l comes from particle coagulation, condensation and evaporation, external particle losses and sources, mathematically expressed as

$$\frac{\mathrm{d}Q_l}{\mathrm{d}t} = \left.\frac{\mathrm{d}Q_l}{\mathrm{d}t}\right|_{coag} + \left.\frac{\mathrm{d}Q_l}{\mathrm{d}t}\right|_{cond-evap} + \left.\frac{\mathrm{d}Q_l}{\mathrm{d}t}\right|_{exter\ loss} + \left.\frac{\mathrm{d}Q_l}{\mathrm{d}t}\right|_{exter\ source} \tag{8}$$

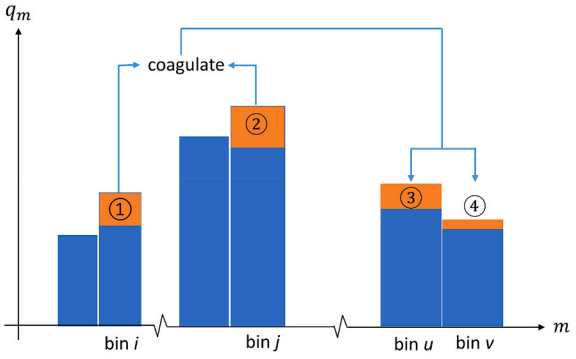

Fig. 2. A graphical illustration of particle coagulation. Particles from bin i and bin j coagulate and the coagulation products go into bin u and bin v.

In the following we will discuss the calculation details for $\left.\frac{dQ_i}{dt}\right|_{coag}$, $\left.\frac{dQ_i}{dt}\right|_{cond-evap}$, $\left.\frac{dQ_i}{dt}\right|_{exter\ loss}$ but not $\left.\frac{dQ_i}{dt}\right|_{exter\ source}$, since external particle sources are very specific to individual aerosol systems and are difficult to generalize.

2.3.1. Coagulation

The physical picture of coagulation is simple - when two particles collide, they irreversibly merge into a new particle. Particles from any two bins (or from the same bin) can coagulate; here we consider coagulation between particles from bin i and particles from bin j ($2 \le i \le j$) without losing generality. We do not consider monomers in this section as they will be discussed in 2.3.2. The coagulation process is graphically illustrated in Fig. 2. We divide the calculation into two steps: in *step 1*, we shall calculate the yellow areas ① and ②, which indicate the mass of the particles that participate in coagulation between bin i and bin j per unit time; in *step 2,* we will decide which bins the coagulation products goes into and how to redistribute the particle mass among these bins, i.e. we calculate yellow areas ③ and ④.

2.3.1.1. Step 1. We denote the particulate mass in bin i that coagulate with particles from bin j per unit time by $\dot{Y}_{ij}$ (i.e. area ① in Fig. 2). Utilizing Eq. (5), $\dot{Y}_{ij}$ is given by

$$\dot{Y}_{ij} = \int_{S_{j-1}}^{S_j}\int_{S_{i-1}}^{S_i} \beta(x,y) n_x n_y \cdot x \mathrm{d}x\mathrm{d}y = \int_{S_{i-1}}^{S_i}\int_{S_{j-1}}^{S_j} \beta(x,y) \frac{Q_i}{xL_i}\cdot\frac{Q_j}{yL_j}\cdot x \mathrm{d}x\mathrm{d}y = Q_iQ_j \int_{S_{i-1}}^{S_i}\int_{S_{j-1}}^{S_j} \boldsymbol{\beta}(\boldsymbol{x},\boldsymbol{y}) \frac{1}{\boldsymbol{yL_iL_j}} \mathbf{dxdy} \text{ if bin } i \text{ and bin } j \text{ are both sections,} \tag{9a}$$

$$\dot{Y}_{ij} = \int_{S_{j-1}}^{S_j} \beta(i,y) N_i n_y \cdot i \mathrm{d}y = Q_iQ_j \int_{S_{i-1}}^{S_i}\int_{S_{j-1}}^{S_j} \boldsymbol{\beta}(\boldsymbol{i},\boldsymbol{y}) \frac{1}{\boldsymbol{yL_j}} \mathbf{dy}, \quad \text{if bin } i \text{ is discrete, and bin } j \text{ is a section,} \tag{9b}$$

$$\dot{Y}_{ij} = \beta(i,j) N_i N_j \cdot i = Q_iQ_j \cdot \frac{\boldsymbol{\beta}(\boldsymbol{i},\boldsymbol{j})}{\boldsymbol{j}}, \text{if bin } i \text{ and bin } j \text{ are both discrete,} \tag{9c}$$

where $\beta(x,y)$ is the collision rate frequency function ($cm^3\ s^{-1}$) for x-mer and y-mer. In Eq. (9a), $\beta(x,y)n_xn_y$ is the collision rate ($cm^{-3}\ s^{-1}$) between x-mer and y-mer and $\cdot x$ means each of these collisions will cause bin i to lose a mass of x. $\dot{Y}_{ji}$ (area ②) can be calculated in a similar fashion, but one should note in general $\dot{Y}_{ij} \neq \dot{Y}_{ji}$. Eqs. (9a-c) can all be written in the form $\dot{M}_{ij} = Q_iQ_ja_{ij}$, with the expressions for a_{ij} printed in bold. We can assemble all the coefficients a_{ij} into a single matrix to facilitate calculation, as is done in the supplementary MATLAB code.

2.3.1.2. Step 2. We now consider how to assign the coagulation products into the correct bins, i.e. to determine areas ③ and ④. Depending on the discreteness of bin i and bin j, there are three possibilities. Firstly, if bin i and bin j are both discrete, their coagulation products have a single mass - we can put the coagulation products in the correct bin by simply comparing their mass to bin boundaries. Secondly, if bin i is discrete and bin j is sectional, coagulation basically move the particles in bin j by a fixed distance along the mass axis. Since sections grow wider to the right on the mass axis, the coagulation product will end up in less than two bins. Thirdly, if both bin i or bin j are sectional, since an x-mer from bin i and a y-mer from bin j satisfy $S_{i-1} < x \le S_i$ and $S_{j-1} < y \le S_j$, the mass of coagulation products satisfy $S_{i-1} + S_{j-1} < x + y \le S_i + S_j$. It is easy to see that

$$\frac{S_i + S_j}{S_{i-1} + S_{j-1}} = \frac{\kappa\left(S_{i-1} + S_{j-1}\right)}{S_{i-1} + S_{j-1}} = \kappa. \tag{10}$$

Eq. (10) shows the ratio of the upper and lower mass limit of the coagulation products is equal to the section geometric factor. Summarizing our analysis of the three possibilities, we can conclude that with a constant geometric factor, *the coagulation products between any two bins cannot end up in more than two consecutive bins.*

With the above conclusion we assume that the coagulation product of bin i and bin j end up in bin u and bin v. The value of u must satisfy $S_{u-1} \le S_{i-1} + S_{j-1} < S_u$ and v is equal to $u+1$. The mass of the coagulation products that falls into bin u, $\dot{Z}_{ij\to u}$ (area ③), is given by the following integrals

$$\dot{Z}_{ij\to u} = \int_{S_{j-1}}^{S_j}\int_{S_{i-1}}^{S_i} \beta(x,y) n_x n_y \cdot (x+y) \cdot \theta(x+y<S_u) \mathrm{d}x\mathrm{d}y = Q_iQ_j \int_{S_{i-1}}^{S_i}\int_{S_{j-1}}^{S_j} \boldsymbol{\beta}(\boldsymbol{x},\boldsymbol{y}) \frac{(\boldsymbol{x}+\boldsymbol{y})}{\boldsymbol{xyL_iL_j}} \cdot \boldsymbol{\theta}(\boldsymbol{x}+\boldsymbol{y}<\boldsymbol{S_u}) \mathbf{dxdy}, \text{if bin } i \text{ and bin } j \text{ are both sections,} \tag{11a}$$

$$\dot{Z}_{ij\to u} = \int_{S_{j-1}}^{S_j} \beta(i,y) N_i n_y \cdot \theta(i+y<S_u) \mathrm{d}y = Q_iQ_j \int_{S_{j-1}}^{S_j} \boldsymbol{\beta}(\boldsymbol{i},\boldsymbol{y}) \frac{(\boldsymbol{i}+\boldsymbol{y})}{\boldsymbol{iyL_j}} \cdot \boldsymbol{\theta}(\boldsymbol{i}+\boldsymbol{y}<\boldsymbol{S_u}) \mathbf{dy}, \text{ if bin } i \text{ is discrete, and bin } j \text{ is a section,} \tag{11b}$$

$$\dot{Z}_{ij\to u} = \beta(i,j) N_i N_j \cdot (i+j) = Q_iQ_j \cdot \frac{\boldsymbol{\beta}(\boldsymbol{i},\boldsymbol{j})(\boldsymbol{i}+\boldsymbol{j})}{\boldsymbol{ij}}, \text{ if bin } i \text{ and bin } j \text{ are both discrete,} \tag{11c}$$

Because coagulation is mass-conserving, we have $\dot{Z}_{ij\to v} = \dot{Y}_{ij} + \dot{Y}_{ij} - \dot{Z}_{ij\to u}$ (area ④). Similar to Eq. (9), Eq. (11) can also be written in

the form $\dot{Z}_{ij\to u} = Q_i Q_j \boldsymbol{b}_{ij\to l}$, with the expression for $b_{ij\to l}$ printed in bold characters. Finally, $\left.\frac{\mathrm{d}Q_l}{\mathrm{d}t}\right|_{coag}$ is given by

$$\left.\frac{\mathrm{d}Q_l}{\mathrm{d}t}\right|_{coag} = -\sum_{j=2}^{NT}\dot{Y}_{lj} + \frac{1}{2}\sum_{i=2}^{l}\sum_{j=2}^{l}\dot{Z}_{ij\to l} = -\sum_{j=2}^{NT} Q_l Q_j \dot{a}_{lj} + \frac{1}{2}\sum_{i=2}^{l}\sum_{j=2}^{l} Q_i Q_j b_{ij\to l}.(l \geq 2) \tag{12}$$

2.3.2. Condensation and evaporation

We now deal with condensation and evaporation which have been excluded from the previous discussion. In a discrete-sectional framework, condensation/evaporation not only increases/decreases the total particle mass but also causes particle to migrate between neighboring bins. In principle, in an infinitely short duration of time, only particles with masses close to the boundary of two bins need to be considered to calculate inter-sectional mass fluxes induced by condensation/evaporation. However, the boundary discontinuity inherent in the sectional configuration (recall the inset plot in Fig. 1) may cause errors if only the particle concentration at sectional boundaries are used to calculate the mass flux. For a more detailed discussion on such errors, we refer the reader to the work by Warren and Seinfeld (1985). In the following, we apply a method similar to theirs to incorporate condensation/evaporation into our model with 3 steps.

2.3.2.1. Step 1. We first consider condensation and evaporation for particles in a discrete bin l (excluding bin 1 and bin ND). $\left.\frac{\mathrm{d}Q_l}{\mathrm{d}t}\right|_{cond-evap}$ is simply given by

$$\begin{aligned}\left.\frac{\mathrm{d}Q_l}{\mathrm{d}t}\right|_{cond-evap} &= \left.\frac{l\cdot \mathrm{d}N_l}{\mathrm{d}t}\right|_{cond-evap} \\ &= l\cdot[\beta(1,l-1)N_1N_{l-1} - \beta(1,l)N_1N_l - E_lN_l + E_{l+1}N_{l+1}] \\ &= l\cdot\left[\frac{\beta(1,l-1)Q_1Q_{l-1}}{l-1} - \frac{\beta(1,l)Q_1Q_l}{l} - \frac{E_lQ_l}{l} + \frac{E_{l+1}Q_{l+1}}{l+1}\right],\ (2\leq l\leq ND-1)\end{aligned} \tag{13}$$

2.3.2.2. Step 2. We next consider monomer association with particles in a sectional bin l (other than bin ND+1). Assuming a mass accommodation factor of 1 (i.e. all collisions lead to association), the total condensation rate for particles in bin l is given by

$$\int_{S_{l-1}}^{S_l}\beta(1,x)N_1n_x\mathrm{d}x = \int_{S_{l-1}}^{S_l}\beta(1,x)N_1\frac{Q_l}{L_lx}\mathrm{d}x = \boldsymbol{Q}_1\int_{S_{l-1}}^{S_l}\frac{\boldsymbol{\beta}(1,\boldsymbol{x})}{\boldsymbol{L_lx}}\mathbf{dx}\cdot Q_l = \overline{C_l}Q_l \tag{14}$$

where $\overline{C_l}$ is the average coefficient of condensation for section l. Condensation leads to migration of particles from section l to section l+1 and we denote the corresponding mass flux by I_l^+. Since $\overline{C_l}$ is easily calculable (its formula is printed in bold in Eq. (14)), we need to relate I_l^+ to $\overline{C_l}Q_l$. We note that the number of particles that moves out of section l equals the number of particles that moves into section l+1, which leads to

$$-\frac{\overline{C_l}Q_l - I_l^+}{\overline{m}_l} = \frac{I_l^+}{\overline{m}_{l+1}} \tag{15}$$

The left- and right-hand sides of Eq. (15) are the loss and gain of particle number concentrations of section l and l+1 due to inter-sectional mass flux (recall that $\overline{m}_l$ is the average mass of sectional bin l defined in Eq. (7)). Rearranging Eq. (15), the value of I_l^+ is given by

$$I_l^+ = \frac{\overline{C_l}Q_l\overline{m}_{l+1}}{\overline{m}_{l+1}-\overline{m}_l} = \frac{\overline{C_l}Q_l}{1-\frac{1}{\kappa}} \tag{16}$$

Similarly, the total evaporation rate from all particles in bin l in a unit time is given by,

$$\int_{S_{l-1}}^{S_l}E_xn_x\mathrm{d}x = \int_{S_{l-1}}^{S_l}E_x\frac{Q_l}{L_lx}\mathrm{d}x = \int_{S_{l-1}}^{S_l}\frac{\boldsymbol{E_x}}{\boldsymbol{L_lx}}\mathbf{dx}\cdot Q_l = \overline{E_l}Q_l \tag{17}$$

where $\overline{E_l}$ is the average coefficient of evaporation for section l. Evaporation leads to migration of particles from section l to section l-1 and we denote the corresponding mass flux by I_l^-. Again, the number of particles that moves out of section l and the number of particles that moves into section l-1 should be equal, thus we have

$$\frac{\overline{E_l}Q_l + I_l^-}{\overline{m}_l} = \frac{I_l^-}{\overline{m}_{l-1}} \tag{18}$$

The left- and right-hand sides of Eq. (18) are the loss and gain of particle number concentrations of section l and l-1, respectively. Hence, the value of I_l^- is

$$I_l^- = \frac{\overline{E}_l Q_l \overline{m}_{l-1}}{\overline{m}_l - \overline{m}_{l-1}} = \frac{\overline{E}_l Q_l}{\kappa - 1} \tag{19}$$

Putting together equations 14–19, we have

$$\left.\frac{dQ_l}{dt}\right|_{cond-evap} = \overline{C}_l Q_l - I_l^+ + I_{l-1}^+ - \overline{E}_l Q_l - I_l^- + I_{l+1}^-. \ (ND+2 \le l \le NT) \tag{20}$$

2.3.2.3. Step 3. Lastly, we deal with bin 1, bin *ND* and bin *ND*+1. Bin 1 is special in that it exchanges mass with every other bin in the simulation domain. $\left.\frac{dQ_1}{dt}\right|_{cond-evap}$ is given by

$$\left.\frac{dQ_1}{dt}\right|_{cond-evap} = E_2 Q_2 + \sum_{l=3}^{ND} \frac{E_l Q_l}{l} + \sum_{l=ND+1}^{NT} \overline{E}_l Q_l - \sum_{l=1}^{ND} \frac{\beta(1,l) Q_l Q_l}{l} - \sum_{l=ND}^{NT} \overline{C}_l Q_l \tag{21}$$

Bin *ND* and bin *ND*+1 are special because they are at the intersection between discrete and sectional bins. For these two bins we have

$$\left.\frac{dQ_{ND}}{dt}\right|_{cond-evap} = ND \cdot \left[\frac{\beta(1,ND-1) Q_1 Q_{ND-1}}{ND-1} - \frac{\beta(1,ND) Q_1 Q_{ND}}{ND} - \frac{E_{ND} Q_{ND}}{ND}\right] + I_{ND+1}^- \tag{22}$$

and

$$\left.\frac{dQ_{ND+1}}{dt}\right|_{cond-evap} = \overline{C}_{ND+1} Q_{ND+1} - I_{ND+1}^+ + \frac{\beta(1,ND) Q_1 Q_l (ND+1)}{ND} - \overline{E}_{ND+1} Q_{ND+1} - I_{ND+1}^- + I_{ND+2}^- \tag{23}$$

We encourage the reader to try to explain each term in Eqs. 21–23 as a check for understanding.

2.3.3. Particle external losses

The most common external loss mechanisms encountered in box-model simulations are system dilution, particle wall loss and coagulation with pre-existing particles. We will not consider the physics of these processes in detail but refer the reader to McMurry and Li (2017). Each of these processes can be accounted for by a (size-dependent) rate constant, with M for dilution, W_l for wall loss and $CoagS_l$ for coagulation with pre-existing particles. We then have

$$\left.\frac{dQ_l}{dt}\right|_{exter\ loss} = -EL_l Q_l = -(M + W_l + CoagS_l)\, Q_l \tag{24}$$

M, W_l and $CoagS_l$ are usually determined by the experimental or field measurement conditions. CoagS (or CS) is short for coagulation (condensation) sink (Kulmala et al., 2001). Their exact form used in the supplementary MATLAB code is summarized in appendix A.

Through the discussion in 2.3.1–2.3.3., we have completed all the essential building blocks necessary for a functional discrete-sectional code. In the next step we will provide a few test cases to check the validity of our model.

3. Results and discussion

We now use the supplementary MATLAB code to perform a few test cases, with the purposes of these tests summarized in Table 1. All the simulations are done for a species with a molecular mass of $m_1 = 2.4 \times 10^{-25}$ kg (143 amu), a density $\rho = 1.47 \times 10^3$ kg/m^3 at an ambient temperature of 293.15 K and pressure of 1.01×10^5 Pa. In the processing of the simulation results, we assume all the particles are spherical, hence particle mass can be converted directly to particle diameters. In visualizing particle size distributions, it is common practice to plot $dN/d\log_{10}d_p$ as a function of particle diameter d_p. $dN/d\log_{10}d_p$ can be calculated for bin l with

Table 1
Summary of test cases.

Test case	Purpose
1. Mass balance	To do a preliminary check if the encoded equations are balanced
2. The effect of geometric factor	To understand how section width affects simulation accuracy
3. Asymptotic solutions	To test the simulation results against analytical solutions of the GDE under simplifying conditions
4. Molecular cluster growth	To observe how a cluster population starting from a single size evolve over time
5. Self-preserving distribution	To retrieve a solution of the GDE for a coagulating aerosol in the free molecular regime
6. Wall loss and evaporation	To understand the effect of wall loss and evaporation on particle formation

$$\left.\frac{\mathrm{d}N}{\mathrm{d}log_{10}d_p}\right|_{\text{bin } l} = \frac{N_l}{log_{10}\left[\frac{6m_1(l+0.5)}{\pi\rho}\right]^{\frac{1}{3}} - log_{10}\left[\frac{6m_1(l-0.5)}{\pi\rho}\right]^{\frac{1}{3}}} = \frac{N_l}{\frac{1}{3}log_{10}\left(\frac{l+0.5}{l-0.5}\right)}, \text{ if bin } l \text{ is discrete} \tag{25a}$$

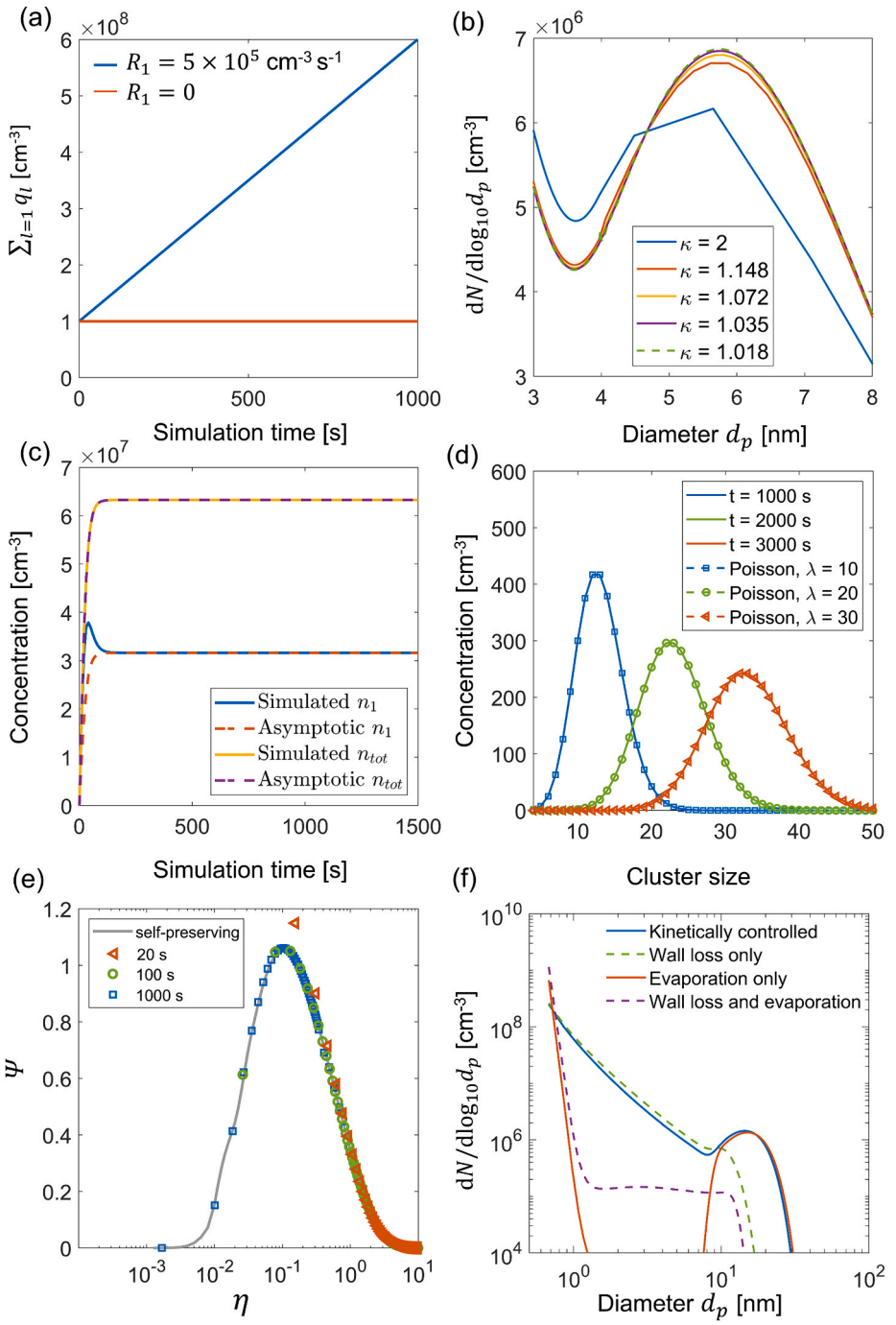

Fig. 3. Simulation results for six test cases: (a) mass balance, (b) the effect of geometric factor, (c) comparison of simulation with asymptotic solutions of the GDE, (d) trimer growth by association with monomers, (e) self-preserving distribution in the free molecular regime, (f) the effect of wall loss and evaporation on particle size distribution. Refer to the text for more details of each test.

$$\left.\frac{\mathrm{d}N}{\mathrm{d}log_{10}d_p}\right|_{\text{bin } l} = \frac{N_l}{log_{10}\left[\frac{6m_1S_l}{\pi\rho}\right]^{\frac{1}{3}} - log_{10}\left[\frac{6m_1S_{l-1}}{\pi\rho}\right]^{\frac{1}{3}}} = \frac{N_l}{\frac{1}{3}log_{10}\kappa}, \text{ if bin } l \text{ is sectional} \tag{25b}$$

In Eq. (25a), we assume that discrete bins have a bin width of 1. For comprehensive parameter settings of each test the reader can refer to the MATLAB input scripts in the supplementary material. Additionally, by going through these test cases, we hope that the reader can gain a deeper insight into discrete-sectional simulations of an evolving aerosol. We also encourage the reader to change the simulation parameters for practice and even reconstruct the code for specialized research goals.

3.1. Mass balance

The very first test of a discrete-sectional code should be to examine if the encoded equations are correctly balanced. One way to do so is to check system mass balance without external particle losses. Total system mass $\left(\sum_l q_l,\ l \geq 1\right)$ as a function of time are shown in Fig. 3a for two such simulations, with the monomer production rate R_1 set to 0 and a constant value 5×10^5 cm^{-3} s^{-1} (20 ppqv s^{-1}), respectively (external production rate other than the monomers are zero). Fig. 3a shows that the $\sum_l q_l$ is a either a constant or increases linearly with a slope of 5×10^5 cm^{-3} s^{-1}, indicating that mass is well balanced in these simulations.

3.2. The effect of geometric factor

A known problem of discrete-sectional models is numerical diffusion (Charan, Huang, & Seinfeld, 2019), which is often mitigated by increasing the number of sections utilized for a given simulation domain, i.e. decreasing the section width. In our model, the section width is controlled by the geometric factor, κ. Fig. 3b shows how simulation results vary with κ for a particle formation event proceeding at the collision-controlled limit (McMurry & Li, 2017), i.e. evaporation, particle external loss rates are zero and the sticking probability between colliding entities is 1. The monomer production rate is $R_1 = 2 \times 10^6$ cm^{-3} s^{-1} (80 ppqv s^{-1}). The value of κ is chosen to be 2, 1.148, 1.0718, 1.0353 and 1.0175 such that it takes 1, 5, 10, 20, and 40 bins for the section width to double. Fig. 3b shows that $\kappa = 2$ gives vastly different results from the others, indicating low accuracy of using a large geometric factor. For other κ values, as κ decreases, the simulation results gradually converge. Using a large number of sections can be very costly in some circumstances, e.g. in global scale simulations. However, in this tutorial we are not quite concerned with simulation time, so we adopt $\kappa = 1.0353$ for all the following test cases.

3.3. Asymptotic solutions

Under simplifying conditions, the GDE can be solved to obtain analytical solutions with which we can compare the simulation results. Specifically, with the following assumptions, i.e. a) the monomer is produced at a constant rate R_1, b) all the collision frequency functions have the same value β_0, and c) evaporation and particle loss processes are absent, the monomer concentration n_1 and the total particle number concentration n_{tot} ($n_{tot} = \sum_{i=1}^{\infty} n_i$) can be shown to asymptotically converge to the following expression (McMurry, 1980),

$$n_1 = \frac{n_{tot}}{2} + \frac{R_1 t}{2\cosh^2\left(\frac{t(R_1\beta_0)^{\frac{1}{2}}}{2^{\frac{1}{2}}}\right)} \tag{26}$$

$$n_{tot} = 2^{\frac{1}{2}}\left(\frac{R_1}{\beta_0}\right)^{\frac{1}{2}} \tanh\left(\frac{t(R_1\beta_0)^{\frac{1}{2}}}{2^{\frac{1}{2}}}\right) \tag{27}$$

A simplified proof of Eqs. (26) and (27) are given in appendix B. As shown Fig. 3c, the simulated n_1 and n_{tot} do converge the analytical solutions with $R_1 = 2 \times 10^6$ cm^{-3} s^{-1} (80 ppqv s^{-1}) and $\beta_0 = 1 \times 10^{-9}$ cm^3 s^{-1}.

3.4. Molecular cluster growth

We now consider the growth of molecular clusters by association with monomers. Suppose initially there are clusters of a single size (i.e. all the clusters have the same number of molecules) in a system with a constant monomer concentration. By constraining the parameters in our model, we only allow these clusters to grow by colliding with monomers at a size-independent rate, while excluding cluster-cluster coagulation, evaporation, and external particle losses. After a certain duration of time, what should be the clusters size distribution? It is tempting to think that the clusters will be of the same size as they collide with monomers at the same frequency. However, because of the stochastic nature of particle collisions, the growing clusters will diffuse in the particle size space (Olenius et al., 2018), i.e. the cluster size distribution will not look like a Dirac delta function but will instead resemble a Poisson distribution. The result of such a test is shown in Fig. 3d for an initial population of trimers at a concentration of $n_{3,t=0} = 1 \times 10^4$ cm^{-3} (0.4 ppqv s^{-1}), with a monomer association rate of 1×10^{-2} s^{-1} for clusters of any size. Fig. 3d shows that the simulation results agree perfectly

with the following modified Poisson distribution

$$n_k = n_{3,t=0} \cdot \frac{\lambda^{k-3} e^{-\lambda}}{(k-3)!} \ (k \geq 3) \tag{28}$$

where λ is the expected number of monomer associations for a cluster within the simulation time (calculated by the simulation time t multiplied by 1×10^{-2} s^{-1}), and '$k-3$' accounts for the fact that all clusters starts as trimers. Simulation results at $t = 1000s$, 2000s, 3000s correspond to $\lambda = 10, 20, 30$, respectively.

3.5. Self-preserving distribution

In addition to Eqs. (26) and (27), there is another special solution for the GDE under more realistic conditions, referred to as the self-preserving particle size distribution. Self-preserving means for certain classes of collision frequency functions, a dimensionless form of the particle size distribution function will be reached after sufficiently long times for a coagulating aerosol, regardless of the initial shape of the distribution (Friedlander & Wang, 1966; Lai, Friedlander, Pich, & Hidy, 1972). Here we look at the self-preserving distribution if the collision frequency function is free molecular. With the total particle number concentration $n_{tot} = \sum_{i=1}^{\infty} n_i$ and total particle mass concentration $q_{tot} = \sum_{i=1}^{\infty} q_i$, we define two dimensionless parameters

$$\eta(k) = \frac{k \cdot n_{tot}}{q_{tot}} \tag{29}$$

$$\Psi(k) = \frac{n_k q_{tot}}{n_{tot}^2} \tag{30}$$

The distribution $\Psi(k)$ as a function of $\eta(k)$ at simulation times t = 20s, 100s, and 1000s are shown in Fig. 3e for a system starting with a population of monomers at 1×10^9 cm^{-3}. Evaporation, external particle loss and production are all set to zero in this simulation. Fig. 3e shows that the simulation results approaches the self-preserving distribution given by Graham and Robinson (1976), i.e. the grey curve, as time proceeds. The method used by Graham and Robinson to obtain their solution is somewhat complicated and we refer the reader to their paper for more information.

3.6. Cluster evaporation and wall loss

In the last test case, we will conduct simulations of more practical importance, i.e. we will look at the effect of wall loss and cluster evaporation on particle size distributions. Fig. 3f shows simulation results for four scenarios with the same monomer production rate $R_1 = 2 \times 10^6$ $cm^{-3}s^{-1}$ (80 ppqv s^{-1}) at $t = 3000s$:

(1) The collision-controlled limit. .
(2) Same condition as in (1) but with a wall loss constant of 0.01 for the monomer. For k-mers the wall loss rate scales with $k^{-\frac{1}{3}}$.
(3) Same condition as in (1) but with a dimer evaporation rate of 2.98 s^{-1}. This evaporation rate corresponds to a saturation vapor concentration of 2×10^4 cm^{-3} and a surface tension of 67.5 mN/m at 293 K. Refer to Appendix A for how the evaporation rate varies with cluster size.
(4) Particle wall loss and evaporation coexist, with the same rate constant as in (2) and (3), respectively.

Fig. 3f shows that wall loss reduces the number of large particles and diminishes the local peak compared to the collision-controlled limit. Evaporation, on the other hand, does not diminish the local peak but creates a deep valley in the cluster size distribution due to the high evaporation rate of the small particles. When coupled together, wall loss and evaporation significantly reduce the number concentration of particles. We leave it to the reader to think about why wall loss-evaporation coupling has such a dramatic effect on the particle size distribution (Li & McMurry, 2018).

4. Summary

In this tutorial we present a detailed guide to build up a discrete-sectional code to simulate an evolving aerosol for a unary, homogeneous system. A MATLAB code together with six test cases are provided so that the reader can quickly master the materials and apply them in research. There are many upgrades that can be made to the presented methods for more sophisticated simulations, e.g. incorporating multiple nucleating species(Gelbard & Seinfeld, 1980; Yu et al., 2018), calculating evaporation rates with quantum-mechanical based free energies (McGrath et al., 2012) and coupling GDE with fluid dynamics models (Kommu et al., 2004a; 2004b). We believe this tutorial can serve as a good starting point towards such simulations.

Supplemental information

The MATLAB source code and the simulation results presented in Fig. 3 are available online at https://github.com/chenxi20JT/discrete-sectional-code.

Acknowledgements

Financial support from Academy of Finland (project number 332547) is appreciated. The authors thank Dr. Peter McMurry for the guidance in building the discrete-sectional model.

About this Article

This article is an Editor-Invited Tutorial Article. Tutorial articles, established to commemorate the 50th Anniversary of the Journal of Aerosol Science in 2020, are intended to serve as educational resources for the aerosol research community on state-of-the-art experimental, theoretical, and numerical techniques in aerosol science.

Appendix A. Rate coefficients in the supplementary code

The rate constants for loss to preexisting particle, wall loss, dilution and evaporation are constructed as the **product of a constant and a size-dependent scaling factor**, which are shown in Table A1.

Table A1
Rate constants for particle external loss and evaporation.

Rate coefficients	Constant	Scaling factor	Explanation
Loss to pre-existing particles, $CoagS_k$	$\frac{1}{4}\left(\frac{8k_bT}{\pi\rho v_1}\right)^{\frac{1}{2}}A_F$	$k^{-\frac{1}{2}}$	$\left(\frac{8k_bT}{\pi\rho v_1}\right)^{\frac{1}{2}}$ is the mean thermal speed of the monomer, A_F is the Fuchs surface area, the scaling accounts for change of mean thermal speed as a function of particle size. Note k_b is the Boltzmann constant, k is number of molecules in the particle.
Wall loss, W_k	$C_w(D_1)^{\frac{1}{2}}$	$k^{-\frac{1}{3}}$	C_w is an experimentally determined wall loss constant (Crump & Seinfeld, 1981). D_1 is diffusion coefficient for the monomer, the scaling accounts for the change of diffusion coefficients as a function of particle size.
Dilution, M	$\frac{Q_{dil}}{V_{chamber}}$	1	Dilution rate is independent of particle size. In a chamber experiment, $V_{chamber}$ is the volume of a chamber, Q_{dil} is the dilution flow rate.
Evaporation rate, E_k $(k \geq 2)$	n_{sat}	$\beta(1,k-1)\exp\left(\frac{3}{2}A\left(k^{\frac{2}{3}}-(k-1)^{\frac{2}{3}}\right)\right)$	See text below for the derivation

A simple explanation of the evaporation rate in Table A1 is as follows. In a *saturated* vapor at equilibrium, the forward and backward rate of the following reaction is the same

$$(k-1)-\text{mer}+\text{monomer} \Leftrightarrow k-\text{mer}\ (k \geq 2). \tag{R1}$$

If we assume unit sticking probability of monomer as monomers and k-mers collide, we have

$$\beta(1,k-1)n_{k-1,s}n_{sat} = E_k n_{k,s}, \tag{A1}$$

where n_{sat} is the saturated vapor concentration. At equilibrium, law of mass action leads to

$$\frac{\frac{n_{k,s}}{n_{sat}}}{\frac{n_{k-1,s}}{n_{sat}}\cdot\frac{n_{sat}}{n_{sat}}} = \exp\left(-\frac{\Delta G^*_{k-1\to k}}{kT}\right), \tag{A2}$$

where $\Delta G^*_{k-1\to k}$ is the free energy change of the reaction (R1), $n_{k,s}$ is the equilibrium number concentration of k-mers. Combining Eq. (A1) and (A2), we have

$$E_k = \beta(1,k-1)n_{sat}\exp\left(\frac{\Delta G^*_{k-1\to k}}{kT}\right) = \beta(1,k-1)n_{sat}\exp\left(\frac{3}{2}A\left(k^{\frac{2}{3}}-(k-1)^{\frac{2}{3}}\right)\right), \tag{A3}$$

where $\Delta G^*_{k-1\to k}$ is calculated by the surface energy change from (*k-1*)-mer to *k*-mer with bulk properties of the nucleating species. *A* is the dimensionless surface tension, given by

$$A = 4\left(\frac{\pi}{6}\right)^{\frac{1}{3}}(v_1)^{\frac{2}{3}}\frac{\sigma}{k_b T}, \tag{A4}$$

where σ is the bulk surface tension. $\Delta G^*_{k-1\to k}$ in Eq. (A2) can be calculated for small clusters by more advanced methods, e.g. quantum mechanical calculations.

Appendix B. A brief proof of Eqs. (26) and (27)

Here we give a brief outline of how Eqs. (26) and (27) are derived. Under the assumptions given in section 3.3, we have

$$\frac{dn_1}{dt} = R \quad - \beta_0 n_1 \sum_{j=1}^{\infty} n_j = R - \beta_0 n_1 n_{tot}, \tag{B1}$$

$$\frac{dn_k}{dt} = \frac{1}{2}\sum_{i+j=k}\beta_0 n_i n_j \quad - \beta_0 n_k \sum_{j=1}^{\infty} n_j = \frac{1}{2}\sum_{i+j=k}\beta_0 n_i n_j - \beta_0 n_k n_{tot}. \tag{B2}$$

Summing up the equations for the monomer and all the clusters leads to

$$\frac{dn_{tot}}{dt} = R + \frac{1}{2}\beta_0 \sum_{k=2}^{\infty}\sum_{i+j=k} n_i n_j - \beta_0 n_{tot}^2. \tag{B3}$$

Recognizing that $\sum_{k=2}^{\infty}\sum_{i+j=k} n_i n_j = n_{tot}^2$, we have

$$\frac{dn_{tot}}{dt} = R - \frac{1}{2}\beta_0 n_{tot}^2 \tag{B4}$$

Solving Eq. (B4) gives Eq. (27). Substituting Eq. (27) into Eq. (B1) leads to Eq. (26).

References

Charan, S. M., Huang, Y., & Seinfeld, J. H. (2019). Computational simulation of secondary organic aerosol formation in laboratory chambers. *Chemical Reviews, 119* (23), 11912–11944. https://doi.org/10.1021/acs.chemrev.9b00358.

Chen, M., Titcombe, M., Jiang, J., Jen, C., Kuang, C., Fischer, M. L., et al. (2012). Acid–base chemical reaction model for nucleation rates in the polluted atmospheric boundary layer. *Proceedings of the National Academy of Sciences, 109*(46), 18713. https://doi.org/10.1073/pnas.1210285109.

Crump, J. G., & Seinfeld, J. H. (1981). Turbulent deposition and gravitational sedimentation of an aerosol in a vessel of arbitrary shape. *Journal of Aerosol Science, 12* (5), 405–415. https://doi.org/10.1016/0021-8502(81)90036-7.

Friedlander, S. K., & Wang, C. S. (1966). The self-preserving particle size distribution for coagulation by brownian motion. *Journal of Colloid and Interface Science, 22* (2), 126–132. https://doi.org/10.1016/0021-9797(66)90073-7.

Gelbard, F., & Seinfeld, J. H. (1979). The general dynamic equation for aerosols. Theory and application to aerosol formation and growth. *Journal of Colloid and Interface Science, 68*(2), 363–382. https://doi.org/10.1016/0021-9797(79)90289-3.

Gelbard, F., & Seinfeld, J. H. (1980). Simulation of multicomponent aerosol dynamics. *Journal of Colloid and Interface Science, 78*(2), 485–501. https://doi.org/10.1016/0021-9797(80)90587-1.

Gelbard, F., Tambour, Y., & Seinfeld, J. H. (1980). Sectional representations for simulating aerosol dynamics. *Journal of Colloid and Interface Science, 76*(2), 541–556. https://doi.org/10.1016/0021-9797(80)90394-X.

Graham, S. C., & Robinson, A. (1976). A comparison of numerical solutions to the self-preserving size distribution for aerosol coagulation in the free-molecule regime. *Journal of Aerosol Science, 7*(3), 261–273. https://doi.org/10.1016/0021-8502(76)90041-0.

Kommu, S., Khomami, B., & Biswas, P. (2004a). Simulation of aerosol dynamics and transport in chemically reacting particulate matter laden flows. Part I: Algorithm development and validation. *Chemical Engineering Science, 59*(2), 345–358. https://doi.org/10.1016/j.ces.2003.05.009.

Kommu, S., Khomami, B., & Biswas, P. (2004b). Simulation of aerosol dynamics and transport in chemically reacting particulate matter laden flows. Part II: Application to CVD reactors. *Chemical Engineering Science, 59*(2), 359–371. https://doi.org/10.1016/j.ces.2003.05.010.

Kruger, C. H., & Vincenti, W. (1965). *Introduction to physical gas dynamics*. John Wlley & Sons.

Kulmala, M., Dal Maso, M., Mäkelä, J. M., Pirjola, L., Väkevä, M., Aalto, P., et al. (2001). On the formation, growth and composition of nucleation mode particles. *Tellus, 53*(4), 479–490. https://doi.org/10.3402/tellusb.v53i4.16622.

Kürten, A., Jokinen, T., Simon, M., Sipilä, M., Sarnela, N., Junninen, H., et al. (2014). Neutral molecular cluster formation of sulfuric acid–dimethylamine observed in real time under atmospheric conditions. *Proceedings of the National Academy of Sciences, 111*(42), 15019. https://doi.org/10.1073/pnas.1404853111.

Kürten, A., Li, C., Bianchi, F., Curtius, J., Dias, A., Donahue, N. M., et al. (2018). New particle formation in the sulfuric acid–dimethylamine–water system: Reevaluation of CLOUD chamber measurements and comparison to an aerosol nucleation and growth model. *Atmospheric Chemistry and Physics, 18*(2), 845–863. https://doi.org/10.5194/acp-18-845-2018.

Lai, F. S., Friedlander, S. K., Pich, J., & Hidy, G. M. (1972). The self-preserving particle size distribution for Brownian coagulation in the free-molecule regime. *Journal of Colloid and Interface Science, 39*(2), 395–405. https://doi.org/10.1016/0021-9797(72)90034-3.

Lehtipalo, K., Rondo, L., Kontkanen, J., Schobesberger, S., Jokinen, T., Sarnela, N., et al. (2016). The effect of acid–base clustering and ions on the growth of atmospheric nano-particles. *Nature Communications, 7*(1), 11594. https://doi.org/10.1038/ncomms11594.

Li, C., & McMurry, P. H. (2018). Errors in nanoparticle growth rates inferred from measurements in chemically reacting aerosol systems. *Atmospheric Chemistry and Physics, 18*(12), 8979–8993. https://doi.org/10.5194/acp-18-8979-2018.

McGrath, M. J., Olenius, T., Ortega, I. K., Loukonen, V., Paasonen, P., Kurtén, T., et al. (2012). Atmospheric cluster dynamics code: A flexible method for solution of the birth-death equations. *Atmospheric Chemistry and Physics, 12*(5), 2345–2355. https://doi.org/10.5194/acp-12-2345-2012.

McMurry, P. H. (1980). Photochemical aerosol formation from SO2: A theoretical analysis of smog chamber data. *Journal of Colloid and Interface Science, 78*(2), 513–527. https://doi.org/10.1016/0021-9797(80)90589-5.

McMurry, P. H., & Li, C. (2017). The dynamic behavior of nucleating aerosols in constant reaction rate systems: Dimensional analysis and generic numerical solutions. *Aerosol Science and Technology, 51*(9), 1057–1070. https://doi.org/10.1080/02786826.2017.1331292.

Olenius, T., Pichelstorfer, L., Stolzenburg, D., Winkler, P. M., Lehtinen, K. E. J., & Riipinen, I. (2018). Robust metric for quantifying the importance of stochastic effects on nanoparticle growth. *Scientific Reports, 8*(1), 14160. https://doi.org/10.1038/s41598-018-32610-z.

Seinfeld, J. H., & Pandis, S. N. (2016). *Atmospheric chemistry and physics: From air pollution to climate change* (3rd ed.). John Wiley & Sons.

Vuollekoski, H., Sihto, S. L., Kerminen, V. M., Kulmala, M., & Lehtinen, K. E. J. (2012). A numerical comparison of different methods for determining the particle formation rate. *Atmospheric Chemistry and Physics, 12*(5), 2289–2295. https://doi.org/10.5194/acp-12-2289-2012.

Warren, D. R., & Seinfeld, J. H. (1985). Simulation of aerosol size distribution evolution in systems with simultaneous nucleation, condensation, and coagulation. *Aerosol Science and Technology, 4*(1), 31–43. https://doi.org/10.1080/02786828508959037.

Wu, C. Y., & Biswas, P. (1998). Study of numerical diffusion in a discrete-sectional model and its application to aerosol dynamics simulation. *Aerosol Science and Technology, 29*(5), 359–378. https://doi.org/10.1080/02786829808965576.

Wu, J. J., & Flagan, R. C. (1988). A discrete-sectional solution to the aerosol dynamic equation. *Journal of Colloid and Interface Science, 123*(2), 339–352. https://doi.org/10.1016/0021-9797(88)90255-X.

Yu, F., Nadykto, A. B., Herb, J., Luo, G., Nazarenko, K. M., & Uvarova, L. A. (2018). H_2SO_4–H_2O–NH_3 ternary ion-mediated nucleation (TIMN): Kinetic-based model and comparison with CLOUD measurements. *Atmospheric Chemistry and Physics, 18*(23), 17451–17474. https://doi.org/10.5194/acp-18-17451-2018.

Chenxi Li received a BEng in Engineering Physics at Tsinghua university. He obtained his PhD at the University of Minnesota in mechanical engineering. He is currently an assistant professor at Shanghai Jiao Tong University. His research interest mainly lies in gas phase nucleation and particle growth, aerosol system dynamics, and analytical techniques including ion-mobility-mass spectrometry.

Runlong Cai received a BS degree and a PhD in environmental science and engineering at Tsinghua University. He is currently a postdoctoral researcher at the University of Helsinki. His research is focused on the physical and chemical properties of atmospheric clusters and new particles.